

Sensitivity of a Coupled Ocean–Atmosphere Model to Physical Parameterizations

CHUNG-CHUN MA, CARLOS R. MECHOSO, AKIO ARAKAWA, AND JOHN D. FARRARA

Department of Atmospheric Sciences, University of California, Los Angeles, Los Angeles, California

(Manuscript received 27 August 1993, in final form 2 March 1994)

ABSTRACT

The sensitivity of a coupled ocean–atmosphere general circulation model to parameterizations of selected physical processes is studied. The parameterizations include those of longwave radiation and surface turbulent fluxes in the atmospheric model, and those of vertical turbulent mixing and penetration of solar radiation in the ocean model. It is shown that the performance of the coupled model is highly sensitive to the parameterization of longwave radiation. This sensitivity is not solely due to the difference in surface radiative flux but involves interactions among radiation, convection, and large-scale dynamics of the atmosphere and ocean. It is concluded that differences in parameterizations can have large impacts on the performance of the coupled model, and these impacts can be very different from what may be expected from uncoupled model simulations.

1. Introduction

The study of phenomena such as El Niño–Southern Oscillation (ENSO) requires consideration of the dynamics and thermodynamics of the coupled ocean–atmosphere system. Coupled general circulation models (GCMs), consisting of an atmospheric GCM (AGCM) exchanging boundary conditions with an oceanic GCM (OGCM), should be ideal tools to study the ocean–atmosphere system. Both components include state-of-the-art parameterizations of physical processes and the coupling allows for the feedback between processes in the two components as well as interactions among processes inside either component.

AGCMs and OGCMs with prescribed boundary conditions at the ocean–atmosphere interface have been used for decades and have been shown to produce simulations that are realistic in many respects. It is not guaranteed, however, that an AGCM coupled to an OGCM will produce simulations of the atmospheric and oceanic circulations of comparable quality to those obtained with the individual components when uncoupled. The reason is that the relaxing of constraints at the ocean–atmosphere interface introduces new degrees of freedom into the system. It comes as no surprise that all present-day coupled GCMs exhibit various degrees of climate drift [i.e., the simulated climatology deviates substantially from that observed (see review by Neelin et al. 1992)]. The climate drift problem in coupled GCMs is currently a major concern in studies of climate and climate variability.

In this paper, we address the climate drift issue by exploring the sensitivity of simulations with a coupled GCM to the parameterizations of selected physical processes. The coupled GCM consists of an AGCM for the global atmosphere and an OGCM for the tropical Pacific Ocean. In the AGCM, the parameterizations we investigate are those of longwave radiative transfer and of fluxes of sensible and latent heat at the surface. In the OGCM, we consider different parameterizations of vertical mixing by turbulence and the impact of penetration of solar radiation in the upper ocean. Our method is based on comparisons between relatively short (generally one year long) integrations with the coupled GCM from identical initial conditions and with different parameterizations of the processes mentioned above. Although one year is admittedly too short to establish the climatology of the coupled ocean–atmosphere system, it is long enough to obtain simulations that differ drastically from each other.

The AGCM and OGCM components of our coupled model are described in section 2. Results from the sensitivity experiments are discussed in section 3. We will show that among the parameterizations of physical processes we have selected to investigate that of longwave radiation has the largest impact on the performance of the coupled model. The reasons for this sensitivity are discussed in section 4. We conclude this paper in section 5 by discussing implications of our findings for the modeling of tropical climate and its variability.

2. The models

The AGCM component of our coupled model is the University of California, Los Angeles (UCLA) AGCM (see Suarez et al. 1983 and references therein). The

Corresponding author address: Dr. Chung-Chun Ma, Department of Atmospheric Sciences, University of California, Los Angeles, 405 Hilgard Ave., Los Angeles, CA 90024-1565.

UCLA AGCM is a finite-difference model that includes sophisticated parameterizations of cumulus convection (Arakawa and Schubert 1974; Lord et al. 1982) and PBL processes (Deardorff 1972; Suarez et al. 1983). The radiation parameterizations are described later in this paper (section 2a). The version of the AGCM used in this study has nine layers in the vertical with the top at 50 mb. The horizontal resolution is 4° in latitude by 5° in longitude. The model includes the diurnal and annual variations of insolation. The AGCM performance is described in several studies (e.g., Randall et al. 1985; Mechoso et al. 1990).

In the version of the AGCM used in this study, a finite timescale is introduced in the cumulus parameterization for the adjustment of the cloud work function (CWF), which is a measure of moist-convective instability, to its quasi-equilibrium value specified for each cloud type. For a given difference of the CWF from the quasi-equilibrium value, this modification reduces the mass flux and, therefore, the tendency of cumulus convection to restore the quasi-equilibrium condition. After a consecutive sequence of these "relaxed adjustments" under a constant forcing from the large-scale environment, the difference between the CWF and its quasi-equilibrium value will be larger (more unstable) compared to the case of instantaneous adjustment, and accordingly, the cumulus parameterization will produce approximately the same mass flux even with the formal reduction of mass flux for a given CWF difference. Thus, the amount of cumulus heating (or cooling) and drying (or moistening), and consequently the amount of cumulus precipitation, hardly changes through this relaxed adjustment. This has been confirmed through actual simulations with the AGCM (Cheng and Arakawa 1993, personal communication). This modification, however, has an important effect on radiation. Since the tendency of cumulus convection to restore the quasi-equilibrium condition is reduced, the lifetime of the simulated convective system becomes longer, which results in a higher cloud incidence and, therefore, larger time-averaged cumulus cloud amount. We have found that simulation of the outgoing longwave radiation is significantly improved with the relaxed adjustment.

The OGCM component of our coupled model is the model developed at the National Oceanic and Atmospheric Administration Geophysical Fluid Dynamics Laboratory/Princeton University (Bryan 1969; Cox 1984). This OGCM is a finite-difference model based on the primitive equations with the Boussinesq approximation. The model uses the rigid-lid assumption to eliminate surface gravity waves that have large phase speeds. The parameterization of vertical mixing by turbulence will be described later in this paper (section 2c).

The OGCM configuration is identical to that of the tropical Pacific OGCM used by Philander and collaborators in several studies of tropical phenomena on the

seasonal and interannual timescales, including ENSO (Philander et al. 1987). In this configuration, the model domain covers the Pacific Ocean from 130°E to 70°W in longitude, and 28°S to 50°N in latitude. In longitude the resolution is 1° . In latitude the mesh size is $1/3^\circ$ between 10°S and 10°N and increases gradually poleward. There are 27 levels in the vertical, with a 10-m resolution in the topmost 10 layers. The model incorporates realistic coastal outlines but has a constant depth of 4149 m. Poleward of both 20°S and 30°N , the temperature and salinity are relaxed toward climatology to minimize the artificial influence of the rigid walls. This OGCM has been shown to be capable of capturing the main features of the 1982/83 El Niño (Philander and Siegel 1985) as well as the seasonal cycle in the tropical Pacific Ocean (Philander et al. 1987) when forced with observational estimates of wind stress.

For the results presented in this paper, the AGCM and OGCM are coupled synchronously by exchanging information every 24 simulated hours. The AGCM is first integrated for one day and then provides the daily-mean wind stress and heat fluxes to the OGCM. The OGCM is integrated for the same day with this forcing and then returns the updated SST to the AGCM. Outside the domain of the OGCM, the SST used in the AGCM is prescribed based on an observed monthly climatology. No ad hoc corrections are applied to the surface fluxes once computed using model fields.

a. Longwave radiative transfer in the atmosphere

Two parameterizations of longwave radiative transfer are available in the current version of the UCLA AGCM: (i) the scheme described by Katayama (1972) and modified by Schlesinger (1976), and (ii) the scheme described by Harshvardhan et al. (1987, 1989). (These schemes will be referred to as the "K" and "H" radiation schemes in this paper.)

The K radiation scheme was developed in the early 1970s for a two-layer version of the UCLA AGCM, and it has been an integral part of several model generations since then. The radiation calculation in the nine-layer version of the AGCM considers only the absorptions by water vapor and carbon dioxide; that in the 15-layer version also includes the absorption by ozone. The K scheme uses weighted-mean transmission functions to simplify the integration over frequency and bulk transmission functions for integration in the vertical column.

The H radiation scheme was developed by Harshvardhan et al. (1987, 1989) for a version of the UCLA AGCM used at the National Aeronautic and Space Administration (NASA) Goddard Space Flight Center (GSFC) and was later incorporated into the UCLA AGCM. The longwave part of this scheme is largely based on the work by Rodgers (1968), Chou and Peng

(1983), and Chou (1984). This radiation scheme considers the absorption by water vapor, carbon dioxide, and ozone in five spectral bands, although the ozone absorption is excluded in the nine-layer version of the AGCM. It also includes the effects of the water vapor continuum, which is considered to play an important role in humid regions such as the Tropics (Ramanathan 1987).

The effect of clouds on radiative transfer is also different in the two radiation schemes. Two types of clouds are included in the UCLA AGCM: 1) cumulus clouds associated with subgrid-scale convection, and 2) clouds associated with grid-scale supersaturation, which includes stratus clouds associated with supersaturation in a sublayer within the PBL (Suarez et al. 1983). Both the K and H schemes incorporate the effects of these two types of clouds in the radiation calculation, except for cumulus below 400 mb. In the K scheme, clouds below 187.3 mb with temperatures warmer than 233 K are considered to be composed of water droplets and have an emissivity of 1. Clouds above 187.3 mb or colder than 233 K are considered to be composed of ice crystals and have an emissivity of 0.5. In the H scheme, the cloud emissivities depend on pressure/thickness and temperature in a prescribed functional form, with different coefficients for cumulus and supersaturation clouds. In most cases, the emissivities of cumulus clouds calculated with the H scheme are larger than those with the K scheme, while the emissivities of supersaturation clouds are generally smaller with the H scheme than with the K scheme, particularly in the upper troposphere.

For the parameterization of shortwave radiative transfer, the scheme based on Katayama (1972) is used in all experiments described in this paper.

b. Sensible and latent heat fluxes at the atmosphere-ocean interface

In the UCLA AGCM the PBL is treated as well mixed and represented by the lowest model layer, whose depth is one of the model's prognostic variables (Suarez et al. 1983). The surface wind stress τ , sensible heat flux F_θ , and moisture flux F_r are calculated in the AGCM using an approach based on the bulk aerodynamic formulas (Suarez et al. 1983):

$$\tau_S = \rho_S C_u^2 |\mathbf{v}_M| v_M, \tag{1a}$$

$$(F_\theta)_S = \rho_S u_* C_\theta (\theta_g - \theta_M), \tag{1b}$$

$$(F_r)_S = \rho_S u_* C_\theta \beta [q^*(T_g) - r_M], \tag{1c}$$

where ρ is air density, $u_*^2 = (\tau/\rho)_S$ is the friction velocity squared, \mathbf{v} is the horizontal wind velocity vector, θ is the potential temperature, q^* is the saturation water vapor mixing ratio, r is the mixing ratio of total water, and T is the temperature. The subscripts S , g , and M indicate values at the surface, ground, and in the PBL,

respectively. The parameter β represents availability of water at the surface and is prescribed in the model version used in this study according to estimates of ground surface properties. In particular, $\beta = 1$ over the ocean. The surface transfer coefficients C_θ and C_u are expressed in terms of the bulk Richardson number and the ratio between the mixed-layer depth and surface roughness (Deardorff 1972). The bulk Richardson number Ri_B is defined as

$$Ri_B = \frac{g}{c_p T_S} \frac{(\delta z)_M (s_{vM} - s_{vg})}{|\mathbf{v}_M|^2}, \tag{2}$$

where g is the acceleration of gravity, c_p is the specific heat at constant pressure, $(\delta z)_M$ is the depth of the PBL, and s_v is the virtual static energy defined as $c_p T_v + gz$, in which T_v is the virtual temperature.

Recent observational studies (Bradley et al. 1990) suggested that the values of C_θ provided by the parameterization are systematically different from those estimated from observational data at low wind speeds. To assess the impact of this discrepancy, we examine the model's sensitivity to a modification in which the minimum wind speed for computing C_θ is 5 m s^{-1} . The wind velocity used to compute the wind stress, and therefore u_* , remains unchanged.

c. Vertical mixing by turbulence in the ocean

Two parameterizations of vertical mixing by subgrid-scale turbulence are available in the OGCM: 1) the first-order closure scheme proposed by Pacanowski and Philander (1981), and 2) the level $2\frac{1}{2}$ second-order closure scheme proposed by Mellor and Yamada (1974, 1982) and implemented as in Rosati and Miyakoda (1988). These schemes will be referred to as the "PP" and "MY" mixing schemes in this paper.

In the PP mixing scheme, the eddy viscosity coefficient K_M and eddy diffusion coefficient K_H are assumed to depend on the Richardson number Ri defined by

$$Ri = \frac{-g \frac{\partial \rho}{\partial z}}{\left(\frac{\partial u}{\partial z}\right)^2 + \left(\frac{\partial v}{\partial z}\right)^2}, \tag{3}$$

where z is the vertical coordinate, ρ is density, and u and v are the eastward and northward velocity components, respectively. The scheme assumes that

$$K_M = \frac{\nu_0}{(1 + \alpha Ri)^n} + \nu_b, \tag{4}$$

$$K_H = \frac{\nu_0}{(1 + \alpha Ri)^{n+1}} + \kappa_b, \tag{5}$$

in which the parameters ν_0 , ν_b , κ_b , n , and α were empirically determined by Pacanowski and Philander (1981) so that the OGCM produces realistic simula-

tions of the tropical oceans. The values we use are similar to those they determined: namely,

$$\begin{aligned} \nu_0 &= 50 \text{ cm}^2 \text{ s}^{-1}, \\ \nu_b &= 0.0134 \text{ cm}^2 \text{ s}^{-1}, \\ \kappa_b &= 0.00134 \text{ cm}^2 \text{ s}^{-1}, \\ n &= 2, \text{ and} \\ \alpha &= 5. \end{aligned} \quad (6)$$

A minimum value of $10 \text{ cm}^2 \text{ s}^{-1}$ is assumed for K_M and K_H in the topmost model layer.

In the MY mixing scheme, the turbulent kinetic energy $b^2/2$ and the turbulence length scale l are prognostic variables governed by the following equations:

$$\begin{aligned} \frac{\partial b^2}{\partial t} + \mathcal{L}(b^2) &= \frac{\partial}{\partial z} \left(K_b \frac{\partial b^2}{\partial z} \right) - 2\overline{w'u'} \frac{\partial u}{\partial z} \\ &\quad - 2\overline{w'v'} \frac{\partial v}{\partial z} - 2 \frac{g}{\rho_0} \overline{w'\rho'} - \frac{2b^3}{B_1 l} + F_b, \end{aligned} \quad (7a)$$

$$\begin{aligned} \frac{\partial b^2 l}{\partial t} + \mathcal{L}(b^2 l) &= \frac{\partial}{\partial z} \left(K_b \frac{\partial b^2 l}{\partial z} \right) \\ &\quad + l E_1 \left[-\overline{w'u'} \frac{\partial u}{\partial z} - \overline{w'v'} \frac{\partial v}{\partial z} - E_3 \left(\frac{g}{\rho_0} \overline{w'\rho'} \right) \right] \\ &\quad - \frac{b^3}{B_1} \left[1 + E_2 \left(\frac{l}{k_0 L} \right)^2 \right] + F_l. \end{aligned} \quad (7b)$$

Here \mathcal{L} is the advection operator

$$\begin{aligned} \mathcal{L}(\mu) &= \frac{1}{a \cos \varphi} \left[\frac{\partial}{\partial \lambda} (u\mu) + \frac{\partial}{\partial \varphi} (v \cos \varphi \mu) \right] \\ &\quad + \frac{\partial}{\partial z} (w\mu) \end{aligned} \quad (8)$$

t is time, λ is longitude, φ is latitude, a is the radius of the earth, w is the vertical velocity component, and ρ_0 is the reference density. Primes denote turbulent quantities and overbars denote ensemble mean; F_b and F_l represent dissipation; k_0 is the von Kármán constant; and E_1, E_2, E_3 , and B_1 are empirical constants (Mellor and Yamada 1982). The parameter L is a measure of the distance from boundaries and is determined by $L^{-1} = |z|^{-1} + |z - z_b|^{-1}$, where z_b is depth of the ocean bottom. The boundary conditions for (7) are

$$b^2 = B_1^{2/3} u_{*o}^2, \quad b^2 l = 0 \quad \text{at } z = 0, \quad (9a)$$

$$b^2 = 0, \quad b^2 l = 0 \quad \text{at } z = z_b, \quad (9b)$$

where $u_{*o} = (|\tau| \rho_0^{-1})^{1/2}$ is the friction velocity. The turbulent fluxes are parameterized as

$$-\overline{w'u'} = K_M \frac{\partial u}{\partial z} \quad (10a)$$

$$-\overline{w'v'} = K_M \frac{\partial v}{\partial z} \quad (10b)$$

$$-\overline{w'\rho'} = K_H \frac{\partial \rho}{\partial z}. \quad (10c)$$

The mixing coefficients are given by

$$K_M = l b S_M \quad (11a)$$

$$K_H = l b S_H \quad (11b)$$

$$K_b = l b S_b, \quad (11c)$$

where S_M, S_H , and S_b are stability parameters determined by the closure assumptions described in Mellor and Yamada (1982).

Ma et al. (1991) compared simulations with the uncoupled OGCM using the two mixing schemes described above. In these simulations, the OGCM was forced with surface wind stress and heat fluxes prescribed as in Philander et al. (1987). It was found that the OGCM with the MY scheme simulates a sharper thermocline in the eastern Pacific along the equator and a slightly deeper equatorial undercurrent core. Otherwise, there were no major differences between the oceanic circulation simulated with the two mixing schemes. Halpern et al. (1994) compared uncoupled OGCM simulations with the two mixing schemes and moored-buoy measurements of temperature and current at 165°E , 140°W , and 110°W on the equator during the period of the 1987 El Niño and 1988 La Niña. The forcing for the OGCM was derived from The Florida State University pseudo-stress and the surface air temperature analysis of the European Centre for Medium-Range Weather Forecasts. They did not find large differences between the simulations with the two schemes, although the results with the PP scheme tend to compare slightly better with the moored-buoy measurements at most locations.

d. Penetration of shortwave radiation into the upper ocean

In the usual treatment, heat fluxes at the atmosphere-ocean interface are directly applied to the top layer of the OGCM. We investigate the effect of distributing the solar heating among layers of the OGCM by allowing the solar radiation to penetrate to greater depths. The downward solar radiation I reaching different depths is parameterized according to the formula given by Paulson and Simpson (1977):

$$I(z) = I(0) [R \exp(z/\zeta_1) + (1 - R) \exp(z/\zeta_2)]. \quad (12)$$

The parameters ζ_1, ζ_2 , and R in (12) depend on the turbidity of water. Since there is no variable in the

OGCM representing ocean turbidity, we chose for (12) the parameters corresponding to clear water (type I) in Jerlov's (1968) classification—namely, $\zeta_1 = 0.35$ m, $\zeta_2 = 23$ m, and $R = 0.58$. With the vertical resolution used in this study, 27% of solar radiation can penetrate the uppermost layer of the OGCM, which is 10 m thick.

3. Sensitivity experiments with the coupled GCM

In this section we study the sensitivity of the coupled GCM to the parameterizations described in the previous section. The procedure followed is based on comparisons of simulations performed with different parameterizations from identical initial conditions. For the AGCM the initial conditions correspond to 15 January in a long-term simulation using the Katayama radiation scheme with prescribed time-varying climatological SST. For the OGCM the initial conditions correspond to a state of rest with distributions of temperature and salinity representing the January climatology (Levitus 1982). The length of integration for each experiment is one year in most cases.

We shall name these sensitivity experiments using a combination of letters that encapsulates information on the parameterizations used. The first letter in the experiment name indicates the longwave radiation scheme in the AGCM (K for Katayama and H for Harshvardhan et al.); the following two letters indicate the vertical mixing scheme in the OGCM (PP for Pacanowski–Philander and MY for Mellor–Yamada). If surface flux modification at low wind speeds and penetration of solar radiation into the ocean are included, we add lower case letters “w” and “p,” respectively, after a dash. For example, experiment “HPP–wp” uses the Harshvardhan et al. radiation scheme in the AGCM and the Pacanowski–Philander mixing scheme in the OGCM, and includes both the surface flux modification at low wind speeds and the penetration of solar radiation into the upper ocean.

Figure 1 shows the SST distributions in July of the second year obtained in experiments KPP, HPP, KMY, and HMY. The most striking feature in Fig. 1 is that using the K radiation scheme in the AGCM results in unrealistically warm SSTs. Clearly, the entire equatorial Pacific is covered by water with surface temperatures over 28°C. A pool of water warmer than 30°C spreads over the central and eastern Pacific, and there is no evidence of an equatorial cold tongue. Extending the simulation for several more years does not result in more realistic SSTs as the model seems to have locked into an equilibrium state. This indicates that the deficiencies in the simulation are not primarily due to initial adjustments from coupling.

Using the H radiation scheme in the AGCM, on the other hand, produces much more realistic SST distributions. Figures 1b and 1d show values that can be even colder than the observed by about 1–2 K. Nevertheless, the east–west temperature gradient on the

equator is maintained throughout the year, and both the warm pool in the western Pacific and the cold tongue in the eastern Pacific have realistic structures. In July the temperature difference at the equator across the Pacific Ocean is more than 4°C, which is comparable to the observations. The temperature gradient along the equator is weaker in January.

Comparison of the time evolution of SST at the equator in experiments KPP and HPP (Fig. 2) clearly indicates that a severe climate drift takes place in the former experiment. Almost right after the coupled simulation begins, warm water surges eastward and eventually covers most of the central equatorial Pacific Ocean, where temperatures can be higher than 30°C. Consistently, regions of strong convective activity extend from the western to the central Pacific, and surface easterlies decrease in the central Pacific to be gradually replaced by surface westerlies (Fig. 3). Experiment HPP, on the other hand, simulates a realistic seasonal evolution of SST. There is a strengthening of the cold tongue in late July, about two months earlier than in the observed climatology. The pattern of zonal wind stress is reasonably well simulated.

The other notable feature in Fig. 1 is that different parameterizations of vertical mixing in the OGCM have a relatively small impact on the simulated SST field. With either mixing scheme the coupled model develops a severe climate drift when the K radiation scheme is used in the AGCM. Using the H radiation scheme in the AGCM, the coupled model produces slightly colder SSTs in the Northern (summer) Hemisphere subtropics in July with the MY scheme than with the PP scheme.

The choice of vertical mixing scheme has a stronger impact on the simulated vertical thermal structure of the upper ocean. Figure 4 compares temperature cross sections on the equator in April of the second year of experiments HPP and HMY. Compared to the PP mixing scheme, the MY scheme produces a much sharper thermocline, especially in the eastern Pacific. This is similar to the results obtained with the uncoupled OGCM (Ma et al. 1991), but the difference in the coupled model simulations is much more pronounced. In particular, the PP scheme produces a very diffuse thermocline and a shallow and not well-defined mixed layer in the western Pacific. These deficiencies may result in unrealistic sensitivity to surface heating in longer-term simulations. The cross sections of zonal current (Fig. 5) show that the Equatorial Undercurrent has comparable intensity in both experiments and is weaker than the observed. The core of the Equatorial Undercurrent is at about the same depth in both experiments. The surface currents are weaker when the MY scheme is used. The results of Ma et al. (1991) and Halpern et al. (1994) suggest that the PP scheme is capable of producing realistic results in the tropical Pacific in uncoupled OGCM simulations. The less satisfactory performance of the PP scheme in the coupled

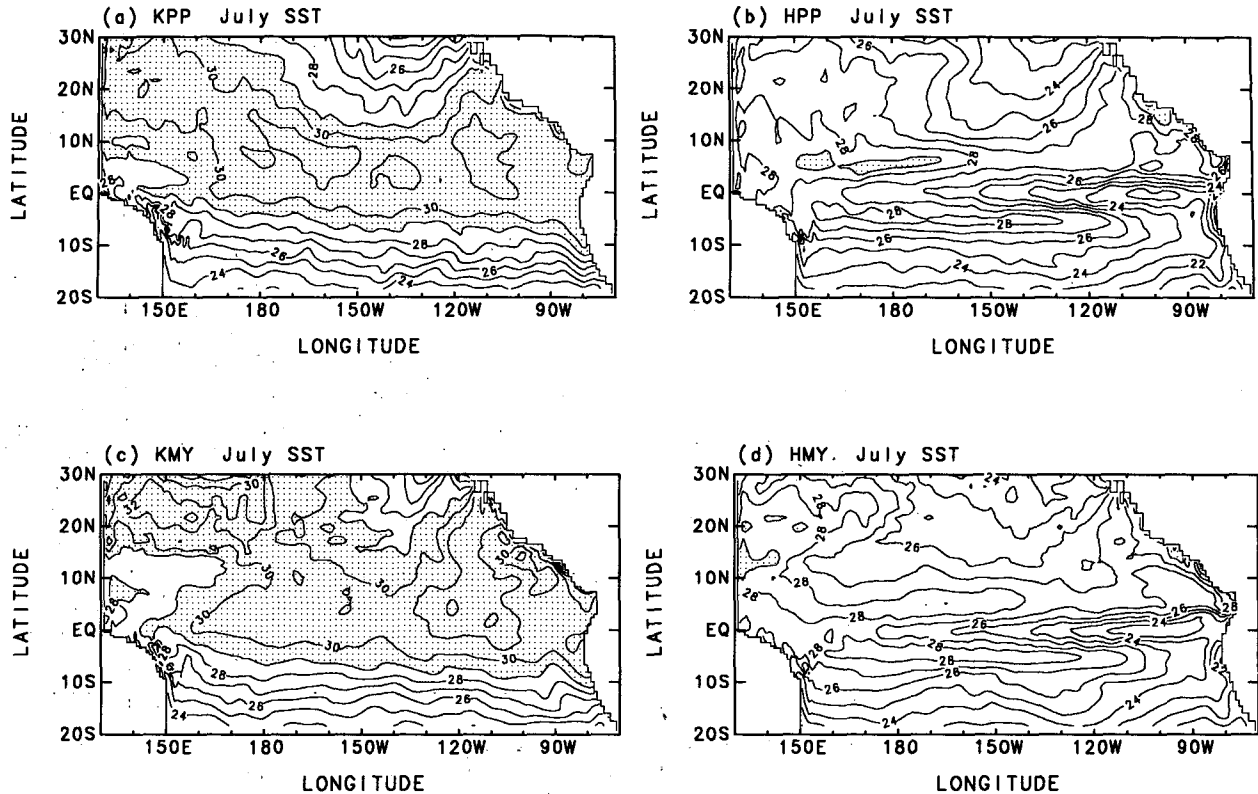


FIG. 1. Sea surface temperature in July of the second year of coupled model integration for experiments (a) KPP, (b) HPP, (c) KMY, and (d) HMY. Contour interval is 1°C . Regions warmer than 29°C are stippled.

simulations can be due, at least in part, to the weak wind stress or excessive heat flux simulated by the AGCM. The MY scheme, on the other hand, is less sensitive to these errors and able to maintain a realistic mixed layer. It is possible that the incorporation of explicit mixed-layer mixing into the PP scheme may alleviate the problem, but it is unclear whether the resulting simulated SST may be too cold.

We next examine the impact on the performance of the coupled GCM of including the modified surface flux calculations at low wind speeds in the AGCM and the penetration of shortwave radiation in the OGCM. Including these two modifications delays the occurrence of the climate drift of the coupled system when the K radiation scheme is used in the AGCM. Nevertheless, the coupled GCM still produces unrealistic SSTs similar to those in Figs. 1a and 1c after one year of integration.

Figure 6 compares the SST distributions obtained in experiments HMY, HMY-p, and HMY-w in July after six months of model integration. Allowing for the penetration of solar radiation into the ocean has an overall cooling effect at the ocean surface. The SSTs are colder by more than 1°C in locations north of 10°N . The difference is largest in the subtropics of the Northern Hemisphere, where the SST is more strongly con-

trolled by the surface heat fluxes and where summer conditions imply larger insolation. Including penetration of solar radiation has a less pronounced and less systematic effect on SSTs in the equatorial belt. At the eastern end of the basin, SSTs are actually warmer when this parameterization is included in the model. The vertical cross sections of temperature along the equator (not shown) reveal that including the penetration of solar radiation produces a sharper thermocline in the central and eastern Pacific.

The modified surface flux calculation at low wind speeds does not have a systematic effect on the SST distribution in the tropical region. It tends to decrease the SST slightly in the western and central Pacific but increase the SST in the cold tongue region.

In summary, we find that the performance of our coupled GCM is highly sensitive to the calculation of longwave radiative transfer in the AGCM. The K scheme, which has been extensively used in the UCLA AGCM, is associated with a severe climate drift that develops from the start of the coupled simulation. The model does not recover from this climate drift even after extending integration for about a decade. The H scheme, which is used in the current version of the UCLA AGCM, produces encouragingly realistic simulations of the climatology and seasonal

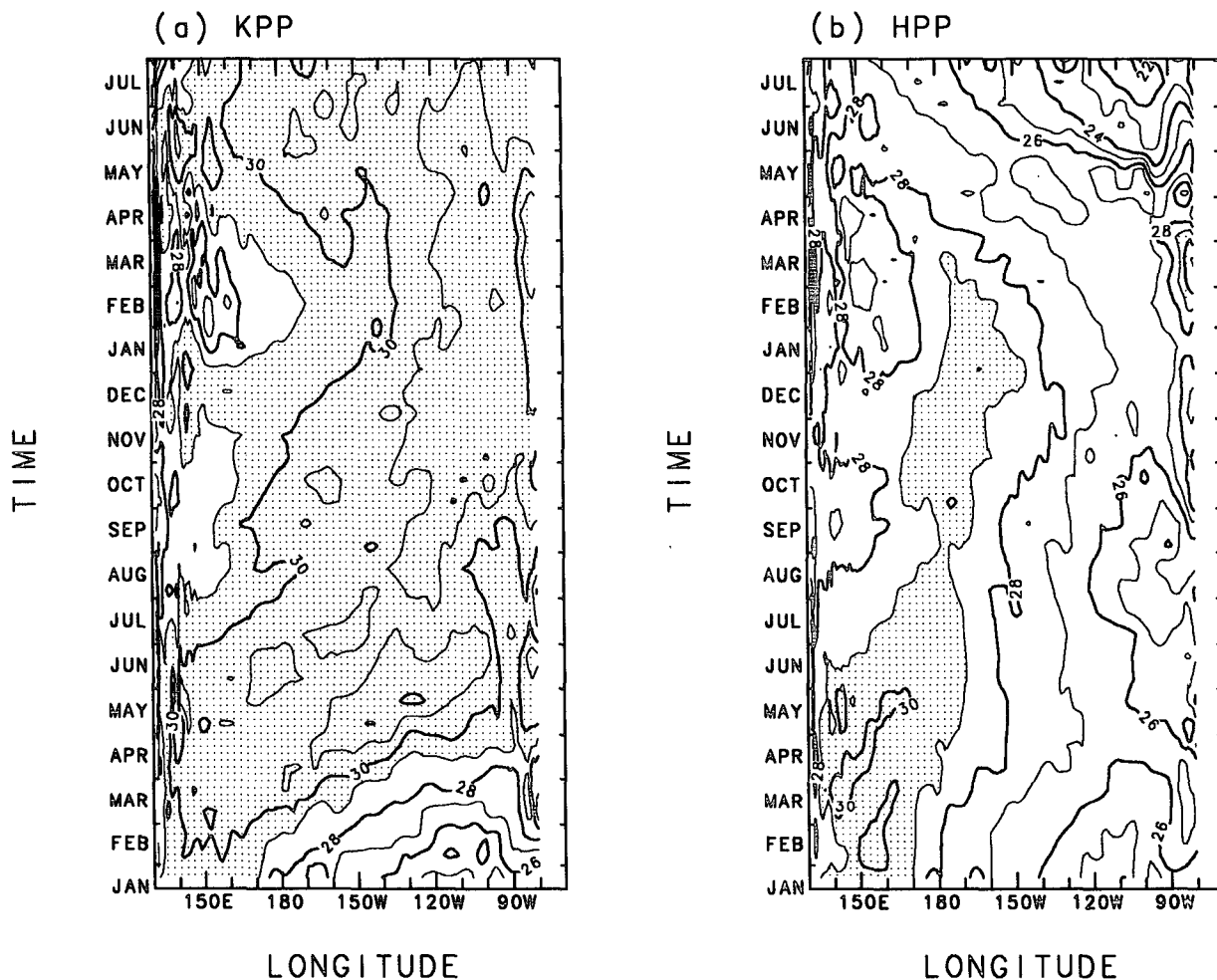


FIG. 2. Longitude-time plots of SST on the equator for experiments (a) KPP and (b) HPP. Contour interval is 1°C. Regions warmer than 29°C are stippled. A 15-day running mean is applied to the data.

cycle in the tropical Pacific region (Robertson et al. 1994a).

4. Interactions among radiation, convection, and large-scale dynamics in the AGCM

In this section we investigate the reasons for the drastic difference between the coupled GCM simulations performed with different parameterizations of longwave radiation in the AGCM. The close relationship between the SST and surface wind stress at the equator shown in the previous section is indicative of feedbacks between the ocean and the atmosphere. These feedbacks involve interactions among surface evaporation, convection, and large-scale dynamics within the AGCM, all of which are linked to the radiative processes. To gain insight into these issues, we analyze the effect of the difference in longwave radiation parameterizations on the atmospheric circulation simulated with the uncoupled AGCM.

The first obvious question is whether the different SST distributions obtained with the two radiation schemes simply reflect different longwave radiative fluxes at the ocean surface. Specifically, we ask whether SSTs are colder with the H scheme because downward longwave radiative fluxes are weaker. In the AGCM, the longwave radiative transfer depends, in a complicated way, on a number of model variables including temperature, water vapor mixing ratio, and cloudiness. As a first step to understand the effect of different longwave radiation schemes, we compare the longwave heating rates and surface longwave radiative fluxes produced by the K and H schemes for *identical* atmospheric conditions. These conditions are produced from a 30-day uncoupled AGCM simulation in perpetual January mode starting from the initial conditions used in the sensitivity experiments described in the previous section. The purpose of the 30-day integration is to produce a more realistic cloud amount with the newly incorporated relaxation in adjustment

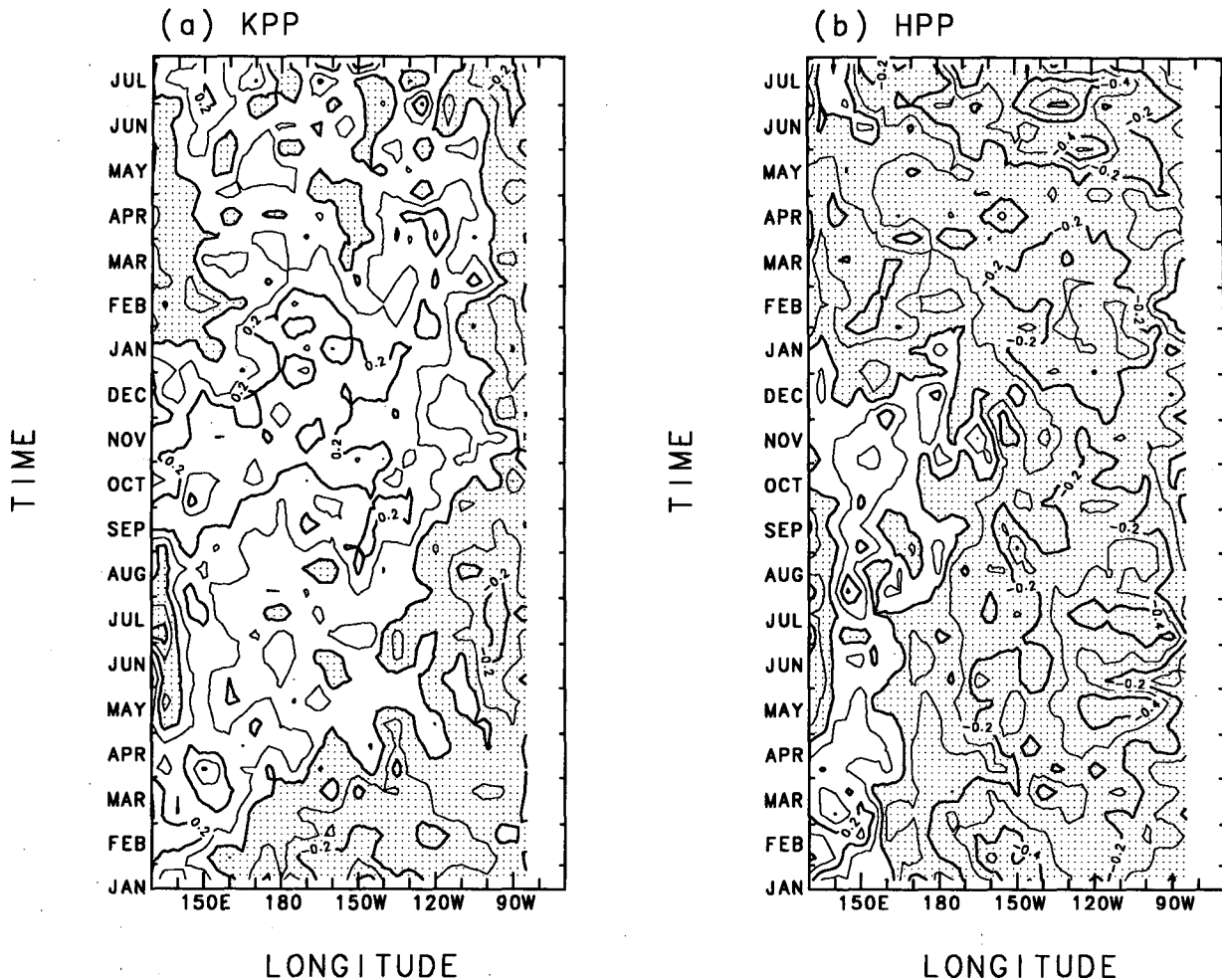


FIG. 3. Longitude-time plots of surface zonal wind stress on the equator for experiments (a) KPP and (b) HPP. Contour interval is 0.1 dyn cm^{-2} ; regions with westward stress are stippled. A 15-day running mean is applied to the data.

by cumulus convection. Figure 7a shows the difference in zonally averaged longwave heating rates produced by the H and K schemes. Since we are primarily interested in the coupled system, the zonal average is taken only over grid points over the ocean.

Figure 7a shows significant differences in the Tropics. Compared to the K radiation scheme, the H radiation scheme produces a stronger cooling both near the surface and in the upper troposphere (around 100 mb). Harshvardhan et al. (1989) compared the heating rates produced by their scheme with and without the effect of the water vapor continuum absorption and found a stronger low-level cooling in the former case. The stronger low-level cooling with the H scheme compared to the K scheme, therefore, can be attributed to the inclusion of continuum absorption in the former scheme. The difference in the upper troposphere, on the other hand, is likely to be associated with differences in the optical properties of clouds assumed in the schemes. To see whether this is the case, we repeat the

longwave heating rate calculation under clear-sky conditions, and the difference is shown in Fig. 7b. Although the H scheme still produces a stronger cooling near the surface, the large differences above 400 mb have disappeared in this case. This supports the hypothesis that different optical properties of clouds are responsible for the stronger upper-level cooling with the H scheme. The reason is that the supersaturation clouds in the upper troposphere, in general, have much smaller emissivities in the H scheme than in the K scheme and thus absorb less of the upward longwave radiation.

The difference in net upward longwave radiative fluxes at the surface computed by the two schemes corresponding to Fig. 7a is shown in Fig. 8. In the Tropics, the net upward flux is smaller with the H scheme, consistent with the stronger downward flux due to emission associated with the water vapor continuum and the stronger cooling at low levels in Fig. 7a. However, this result is in apparent contradiction with the coupled GCM simulations, in which using the H scheme in the

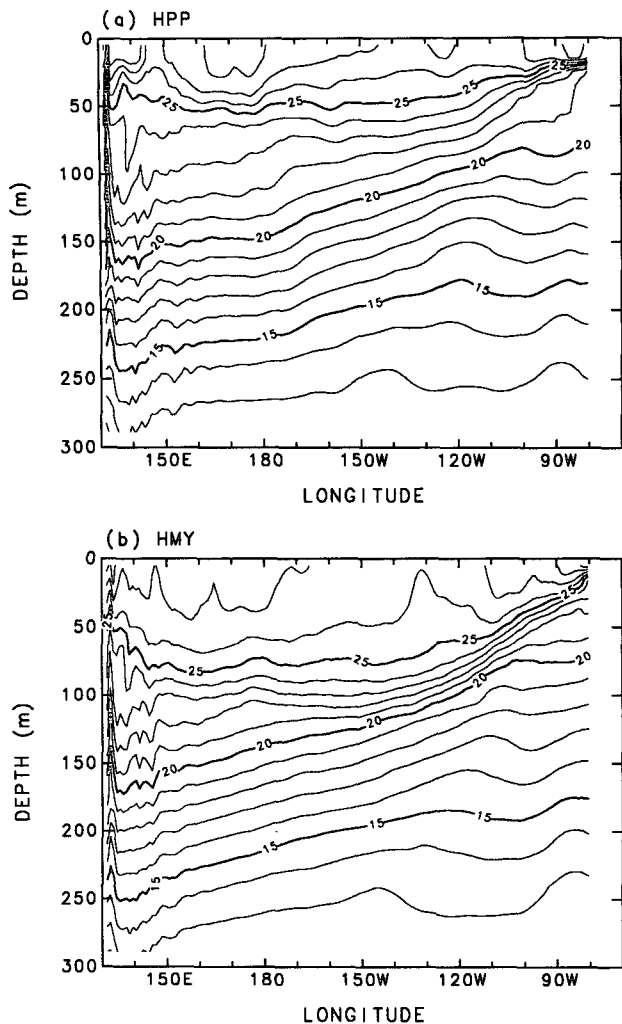


FIG. 4. Cross sections of temperature on the equator in April of the second year of model integration for experiments (a) HPP and (b) HMY. Contour interval is 1°C.

AGCM resulted in *colder* SSTs than using the K scheme. One would expect the net upward longwave radiation to be stronger using the H scheme if the longwave flux alone were to account for the differences in SST. Other surface heat flux components need to be considered, therefore, to account for the behavior of the coupled system.

To this end, we compare the surface heat flux components from two long-term uncoupled AGCM simulations with the two longwave radiation schemes. Specifically, we compare time averages over a 30-day period starting 15 January. Figure 9 shows the differences between zonally averaged surface heat flux components obtained in simulations with the uncoupled AGCM using the H and K schemes. Again, zonal averages are taken over ocean grid points only.

In the Tropics, the net upward longwave radiation (Fig. 9a) is smaller when the H scheme is used. This

tendency toward *weaker* cooling of the ocean with the H scheme is qualitatively similar to that found in the instantaneous calculations. The net downward shortwave radiation (Fig. 9b) is smaller with the H scheme, which implies weaker ocean warming. This difference in shortwave radiation is associated with changes in cloudiness. Since the sensible heat flux has very small magnitudes in the Tropics in the two simulations compared, so does their difference (Fig. 9c). The difference in latent heat flux (Fig. 9d), on the other hand, has a much larger magnitude than that of any other component of the surface heat flux. Compared to the simulation with the K scheme, the simulation with the H scheme shows larger evaporative cooling by more than 30 W m^{-2} in the Tropics. The sign of this difference is consistent with the behavior of the coupled GCM: namely, the H radiation scheme results in a stronger

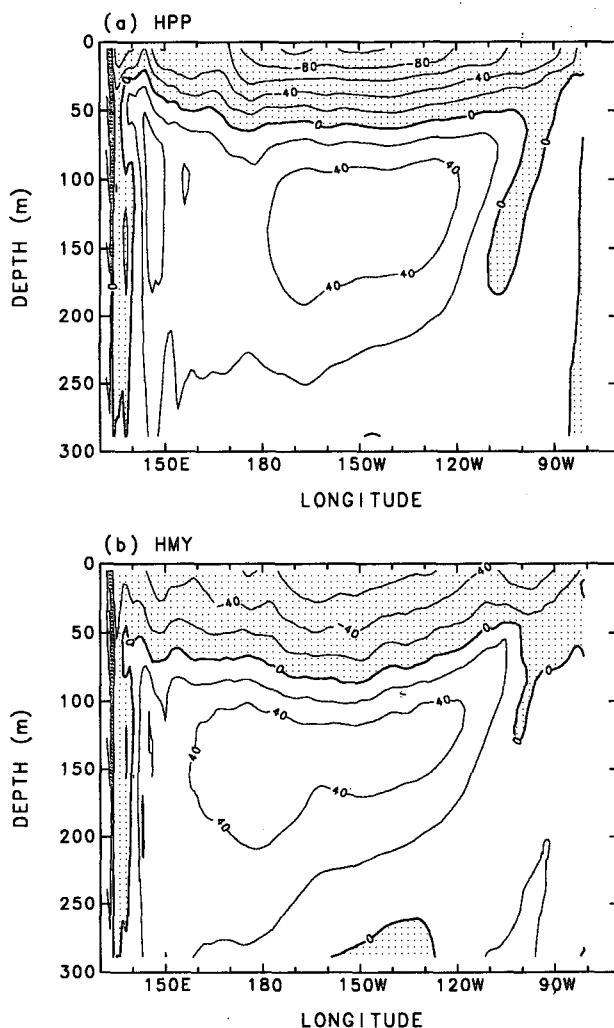


FIG. 5. Cross sections of zonal current on the equator in April of the second year of model integration for experiments (a) HPP and (b) HMY. Contour interval is 20 cm s^{-1} ; regions of westward flow are stippled.

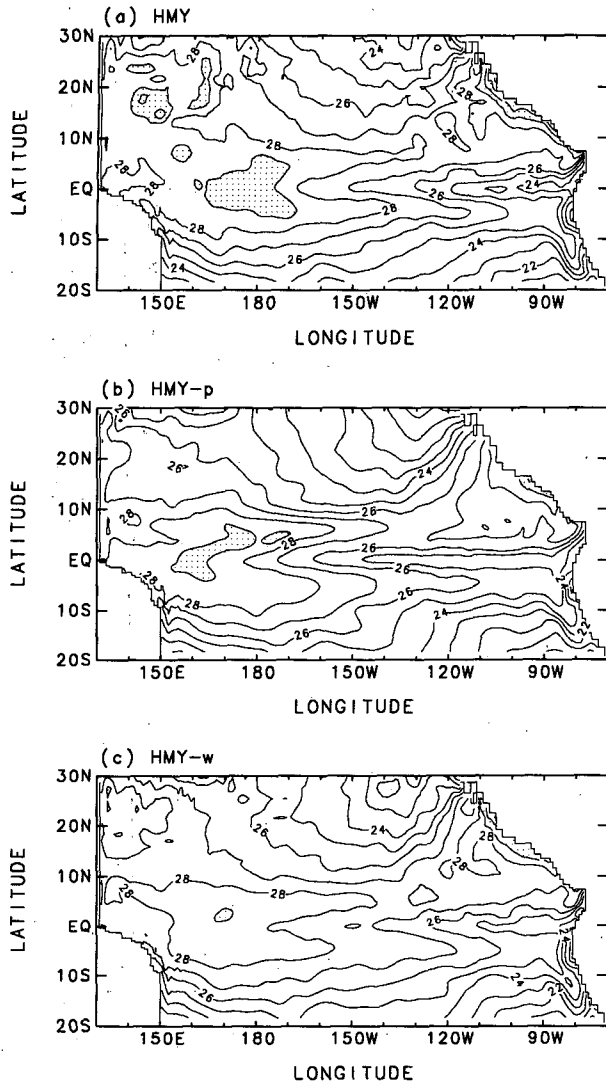


FIG. 6. Simulated sea surface temperature in July of the first year for experiments (a) HMY, (b) HMY-p, and (c) HMY-w. Contour interval is 1°C. Regions warmer than 29°C are stippled.

cooling of the ocean surface. Consistent with the stronger surface evaporation, the total (cumulus and large scale) precipitation is also larger in the simulation with the H scheme (Fig. 9e).

The larger surface evaporation obtained with the H scheme in the uncoupled AGCM is the end result of interactions between radiation, convection, and possibly large-scale dynamics in the model. Recall that for the same atmospheric conditions, the H scheme produces stronger cooling near the surface and in the upper troposphere in the Tropics than the K scheme. A stronger cooling near the surface will enhance the surface heat flux, but more importantly, a stronger upper-level cooling will enhance cumulus activity through destabilization of the atmospheric column. Increased cumulus activity produces more drying of the PBL

through entrainment of drier air from the free atmosphere and, hence, increases surface evaporation.

The changes in convective activity can also interact with large-scale dynamics. The increase in cumulus activity can increase low-level convergence in the Tropics and increase wind speeds in the PBL. The increase in PBL wind speed will also increase surface evaporation.

To quantitatively assess the importance of various processes for the increased surface evaporation in the uncoupled AGCM, we compare the moist static energy flux at the surface in the simulations with the K and H schemes. The moist static energy is given by

$$h = c_p T + gz + Lq, \quad (13)$$

where L is the latent heat of condensation and q is the mixing ratio of total water. The surface moist static energy flux is given by

$$(F_h)_S = \rho_a C_{\theta} u_* (h_g - h_M), \quad (14)$$

where the saturation water vapor mixing ratio at ground temperature is used for q in h_g . A constant

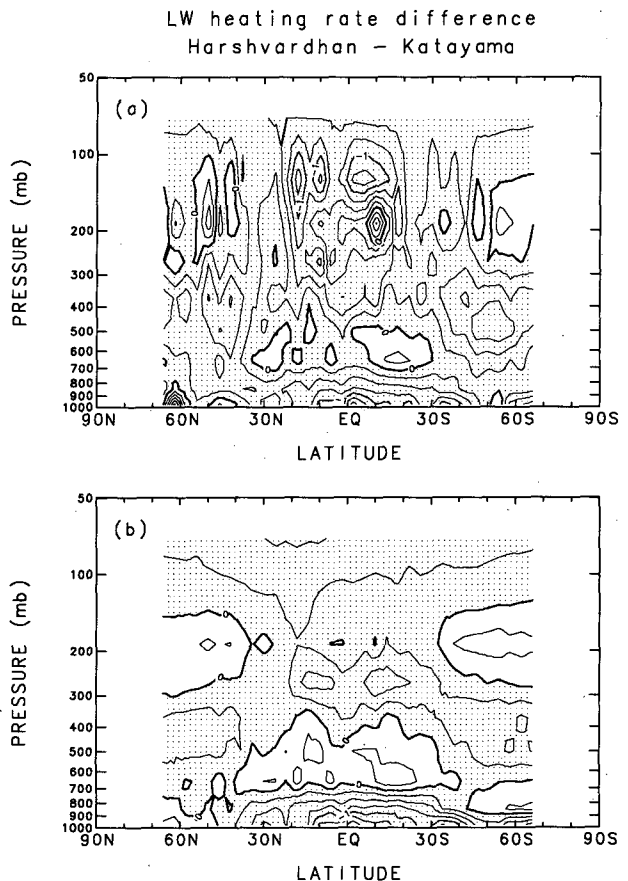


FIG. 7. (a) Difference (Harshvardhan radiation - Katayama radiation) in heating rate due to longwave radiation zonally averaged over ocean grid points for a 15 January condition. Contour interval is 0.25 K day⁻¹. Regions with negative values are stippled. (b) Same as (a) but for clear-sky conditions.

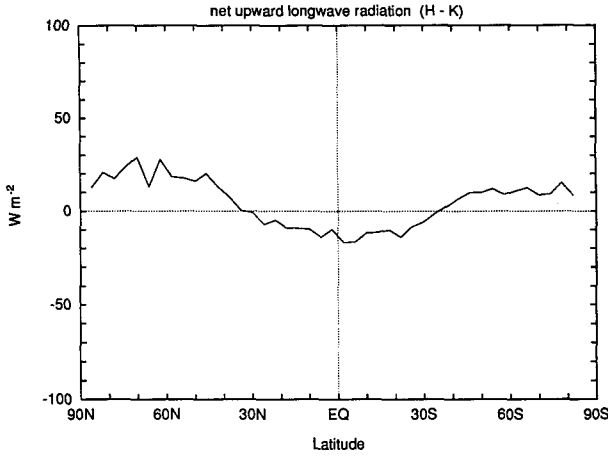


FIG. 8. Difference (Harshvardhan radiation – Katayama radiation) in net upward longwave radiative flux (W m^{-2}) zonally averaged over ocean grid points for a 15 January condition.

value of 1.2 kg m^{-3} is assumed for air density ρ_a . Figure 10a shows the difference in the 30-day mean of surface moist static energy flux zonally averaged over ocean surface (solid line): that is,

$$\Delta(\overline{\rho_a \bar{C}_\theta \bar{u}_* (h_g - h_M)}),$$

where the overbar denotes 30-day mean and Δ denotes the difference between simulations using the H and K schemes. Also shown (dashed line) is the difference in flux computed as the product of the 30-day-mean values of C_θ , u_* , and $h_g - h_M$: that is,

$$\Delta(\rho_a \bar{C}_\theta \bar{u}_* \overline{(h_g - h_M)}).$$

The close agreement between the two curves indicates that the difference in flux can be largely accounted for by the differences in the mean values of individual factors (C_θ , u_* , and $h_g - h_M$) and the higher-order correlation terms in time can be neglected.

We next evaluate the contribution from the three individual factors to the difference in the moist static energy flux by making the following approximation:

$$\begin{aligned} \Delta(\rho_a \bar{C}_\theta \bar{u}_* \overline{(h_g - h_M)}) &\approx \rho_a \Delta(\bar{C}_\theta) (\bar{u}_*)_K \overline{(h_g - h_M)}_K \\ &+ \rho_a (\bar{C}_\theta)_K \Delta(\bar{u}_*) \overline{(h_g - h_M)}_K \\ &+ \rho_a (\bar{C}_\theta)_K (\bar{u}_*)_K \Delta \overline{(h_g - h_M)}, \quad (15) \end{aligned}$$

where subscript K denotes the simulation with the K scheme. The latitudinal distribution of the terms on the right-hand side of (15) is shown in Fig. 10b. It is apparent that in the time-mean changes in the transfer coefficient do not contribute significantly to differences in surface moist static energy flux, whereas changes in u_* and $(h_g - h_M)$ both have nontrivial contributions to the differences. The changes in $(h_g - h_M)$ reflect the colder and drier PBL in the simulation with the H

scheme, which is consistent with the stronger low-level cooling and increased cumulus activity. The changes in u_* are due mainly to changes in the PBL winds and have an even stronger impact on the moist static energy flux in the Tropics than the changes in $(h_g - h_M)$. The surface wind stresses from the two experiments are shown in Fig. 11. It can be clearly seen that the surface wind stress in the simulation with the H scheme is stronger in most places. Most importantly there is much stronger surface convergence in the equatorial region and stronger southeasterly trades in the eastern tropical Pacific. These features indicate enhanced Hadley and Walker circulations, consistent with the enhanced cumulus activity in the western tropical Pacific.

The following scenario for the coupled simulations is suggested by the results discussed in this section. With the K radiation scheme, surface longwave radiative fluxes are not necessarily unrealistic, but the longwave heating rate calculated by this scheme results in vertical temperature distributions that are relatively stable in the Tropics, and, therefore, convective activity is relatively weak. Consequently, surface evaporation and winds are also weak. The insufficient surface evaporative cooling, combined with weak wind stress, leads to unrealistically high SSTs in the coupled model simulation. On the other hand, the H radiation scheme produces a more unstable vertical temperature distribution for the tropical atmosphere and, therefore, stronger convective activity. The stronger surface evaporative cooling and better simulated surface wind stress produce much more realistic SST distributions.

5. Conclusions

We have analyzed the sensitivity of a coupled ocean–atmosphere GCM to the parameterizations of selected physical processes in both the AGCM and the OGCM components of the model. In the AGCM, we focused on the parameterizations of longwave radiative transfer and surface turbulent fluxes at low wind speeds. In the OGCM, we considered the parameterizations of vertical mixing by turbulence and the penetration of solar radiation into the upper ocean.

Among the four physical parameterizations we investigated, the coupled model shows the greatest sensitivity to the parameterization of longwave radiation in the AGCM. This sensitivity is so strong that using one of the schemes considered [the Katayama (1972) scheme, which has been extensively used in the UCLA AGCM] results in a catastrophic climate drift of the model in which unrealistically high SSTs develop in the tropical Pacific, whereas using the other scheme [the Harshvardhan et al. (1987, 1989) scheme, which is used in the current version of the UCLA AGCM] results in a very realistic simulation of the coupled system. Interestingly, the longwave radiation scheme that produces colder SSTs also produces stronger longwave

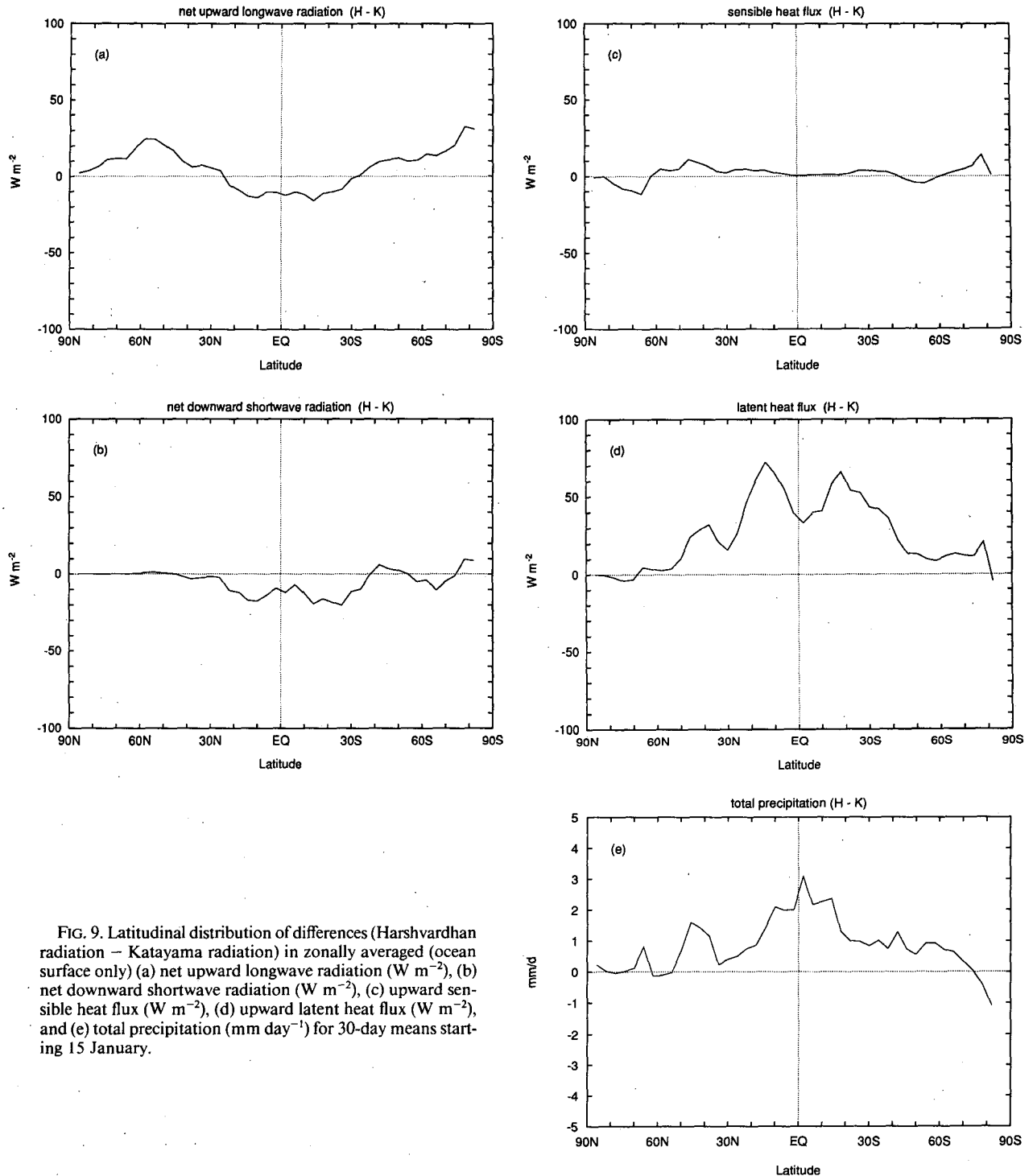


FIG. 9. Latitudinal distribution of differences (Harshvardhan radiation - Katayama radiation) in zonally averaged (ocean surface only) (a) net upward longwave radiation ($W m^{-2}$), (b) net downward shortwave radiation ($W m^{-2}$), (c) upward sensible heat flux ($W m^{-2}$), (d) upward latent heat flux ($W m^{-2}$), and (e) total precipitation ($mm day^{-1}$) for 30-day means starting 15 January.

radiation from the atmosphere into the ocean. Our analyses show that the reason for this apparent contradiction has to be sought in processes other than radiative transfer. It was demonstrated that lower SSTs obtained with the H scheme are due to stronger evaporative cooling of the ocean surface and stronger surface

wind stress in the Tropics, both of which are associated with stronger convective activity.

The other parameterizations we considered do not have as drastic an impact in our coupled model as the longwave radiation parameterization. The two different vertical mixing schemes do not affect the SST signifi-

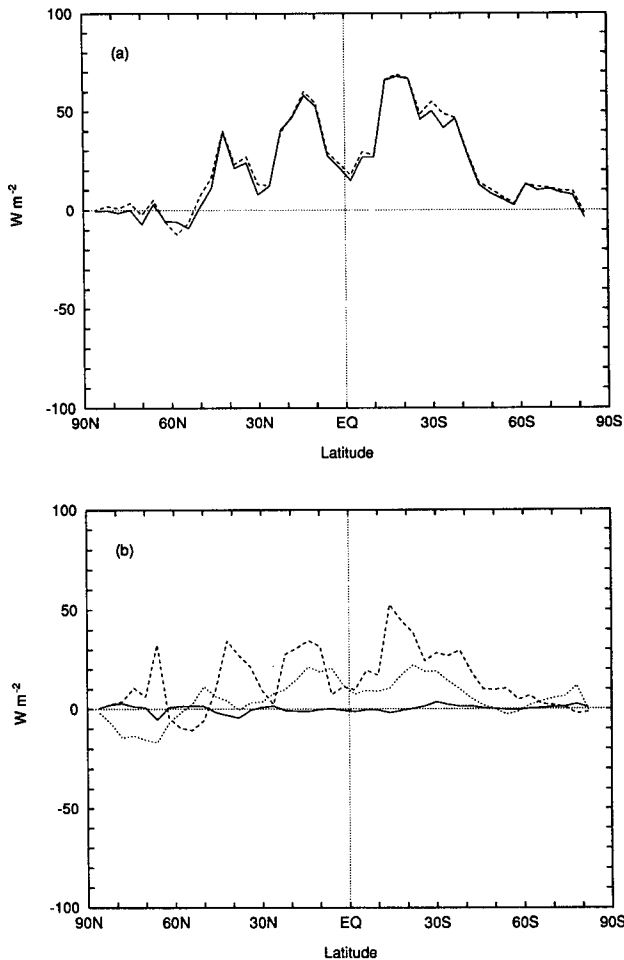


FIG. 10. (a) Difference in surface moist static energy flux (W m^{-2}) for 30-day means starting 15 January (solid line) between simulations with the Harshvardhan et al. and Katayama schemes. The dashed line shows the difference in fluxes computed as the product of 30-day means of individual factors. (b) Contributions of differences in transfer coefficient (solid line), friction velocity (dashed line), and ground-surface moist static energy difference (dotted line) to the difference in surface moist static energy flux.

cantly but strongly influence the structure of the mixed layer and the thermocline. The Pacanowski–Philander parameterization, when used in our coupled model, produces very diffuse thermoclines along the equator and shallow mixed layers in the western equatorial Pacific. The Mellor–Yamada turbulence closure scheme produces more realistic results at those locations. There are indications, however, that the vertical mixing produced by the latter scheme may be too strong.

Our results also demonstrated the sensitivity of SST simulated by the coupled GCM to modification of surface turbulent flux calculations and the penetration of solar radiation into the ocean. Although the resulting differences are small, these slight differences may have a nontrivial impact on the interannual variability of the coupled model (Robertson et al. 1994b).

Our principal finding is that feedbacks in the coupled ocean–atmosphere system imply that coupled GCMs can be highly sensitive to different parameterizations of physical processes. Not only can the sensitivity be much greater in the coupled GCM than that in the model components when uncoupled, but the effect of differences in parameterization schemes in the coupled simulations may also differ drastically from that in the uncoupled simulations. It should be noted, however, that the sensitivity found in this study may be highly dependent upon the resolution and special parameterizations of physical processes used in our current model components. For example, the sensitivity to vertical mixing schemes in the OGCM may be due to the coarseness of vertical resolution. Nevertheless, these considerations do not challenge the major finding of this study: altering a physical parameterization in a

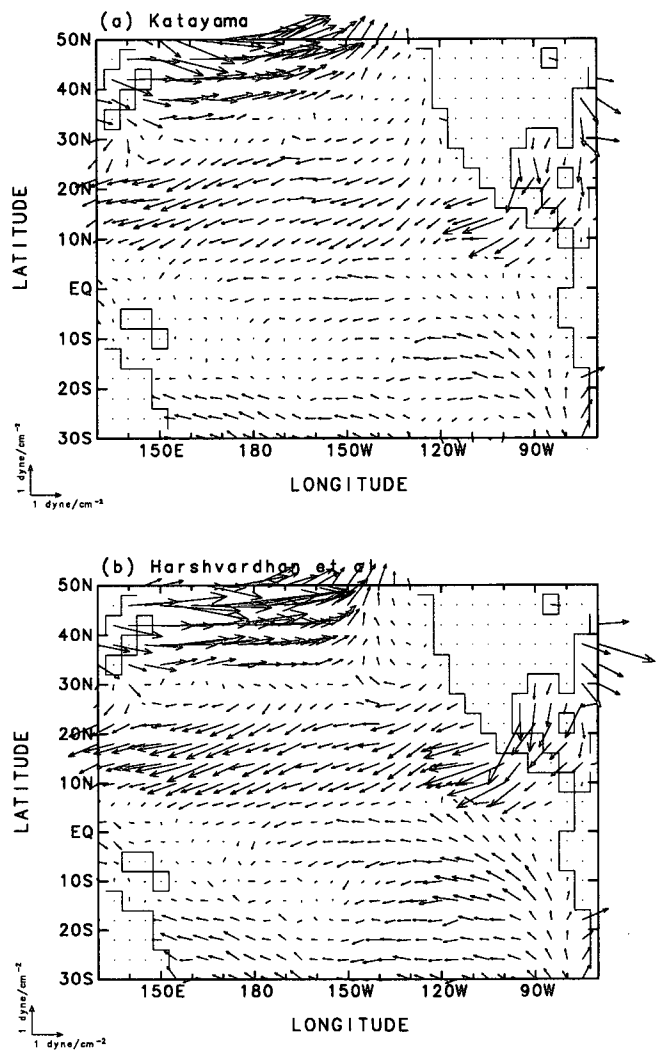


FIG. 11. Thirty-day-mean surface wind stress starting 15 January from uncoupled AGCM simulations using the (a) Katayama and (b) Harshvardhan et al. longwave radiation schemes.

component of a coupled ocean-atmosphere GCM can have large impacts on model performance through the triggering of complicated feedback processes. Careful study and detailed understanding of the interactions among physical parameterizations are crucial for the improvement of coupled model simulations.

Acknowledgments. The authors would like to thank Drs. David A. Randall, J. David Neelin, and Andrew W. Robertson for useful discussions, and Mr. Joseph Spahr for his assistance with the UCLA AGCM. This work was supported by NSF and DARPA under Cooperative Agreement NCR-8919038 with the Corporation for National Research Initiatives and DOE-CHAMMP under Grant DE-FG03-91ER61214. Model integrations were performed at the San Diego Supercomputer Center. Development of the coupled GCM was partially supported by ONR under Grant N00014-89-J-1845.

REFERENCES

- Arakawa, A., and W. H. Schubert, 1974: Interaction of a cumulus cloud ensemble with the large-scale environment. Part I. *J. Atmos. Sci.*, **31**, 674-701.
- Bradley, E. F., J. S. Godfrey, M. Nunez, and P. A. Coppin, 1990: Estimating the total heat flux into the tropical oceans. *Proc. Int. TOGA Scientific Conf.*, World Meteorological Organization, 121-128.
- Bryan, K., 1969: A numerical method for the study of the circulation of the world ocean. *J. Comput. Phys.*, **4**, 347-376.
- Chou, M.-D., 1984: Broadband water vapor transmission functions for atmospheric IR flux computations. *J. Atmos. Sci.*, **41**, 1775-1778.
- , and L. Peng, 1983: A parameterization of the absorption in the 15 μm CO₂ spectral region with application to climate sensitivity studies. *J. Atmos. Sci.*, **40**, 2183-2192.
- Cox, M. D., 1984: A primitive equation, 3-dimensional model of the ocean. GFDL Ocean Group Tech. Rep. No. 1, 143 pp.
- Deardorff, J. W., 1972: Parameterization of the planetary boundary layer for use in general circulation models. *Mon. Wea. Rev.*, **100**, 93-106.
- Halpern, D., Y. Chao, C.-C. Ma, and C. R. Mechoso, 1994: Comparison of Tropical Pacific temperature and current simulations with two vertical mixing schemes embedded in an OGCM and Reference to In Situ Observations. *J. Geophys. Res.*, submitted.
- Harshvardhan, R. Davies, D. A. Randall, and T. G. Corsetti, 1987: A fast radiation parameterization for atmospheric circulation models. *J. Geophys. Res.*, **92**, 1009-1016.
- , D. A. Randall, T. G. Corsetti, and D. A. Dazlich, 1989: Earth radiation budget and cloudiness simulations with a general circulation model. *J. Atmos. Sci.*, **46**, 1922-1942.
- Jerlov, N. G., 1968: *Optical Oceanography*. Elsevier, 194 pp.
- Katayama, A., 1972: A simplified scheme for computing radiative transfer in the troposphere. *Numerical Simulation of Weather and Climate*, Dept. of Meteorology, University of California, Los Angeles, 77 pp.
- Lord, S. J., W. C. Chao, and A. Arakawa, 1982: Interaction of a cumulus cloud ensemble with the large-scale environment. Part IV: The discrete model. *J. Atmos. Sci.*, **39**, 104-113.
- Levitus, S., 1982: *Climatological Atlas of the World Ocean*. NOAA Prof. Paper No. 13, 173 pp. and 17 microfiche.
- Ma, C.-C., Y. Chao, C. R. Mechoso, W. M. Weibel, and D. Halpern, 1991: Comparison of vertical mixing schemes for ocean general circulation models. Preprints, *Fifth Conf. on Climate Variations*, Denver, CO, Amer. Meteor. Soc., 388-391.
- Mechoso, C. R., S. W. Lyons, and J. A. Spahr, 1990: The impact of sea surface temperature anomalies on the rainfall over northeast Brazil. *J. Climate*, **3**, 812-826.
- Mellor, G. L., and T. Yamada, 1974: A hierarchy of turbulence closure models for planetary boundary layers. *J. Atmos. Sci.*, **31**, 1791-1806.
- , and —, 1982: Development of a turbulence closure model for geophysical fluid problems. *Rev. Geophys. Space Phys.*, **20**, 851-875.
- Neelin, J. D., M. Latif, and coauthors, 1992: Tropical air-sea interaction in general circulation models. *Climate Dyn.*, **7**, 73-104.
- Pacanowski, R. C., and S. G. H. Philander, 1981: Parameterization of vertical mixing in numerical models of tropical oceans. *J. Phys. Oceanogr.*, **11**, 1443-1451.
- Paulson, C. A., and J. J. Simpson, 1977: Irradiance measurements in the upper ocean. *J. Phys. Oceanogr.*, **7**, 952-956.
- Philander, S. G. H., and A. D. Siegel, 1985: Simulation of El Niño of 1982-1983. *Coupled Ocean-Atmosphere Models*, J. C. J. Nihoul, Ed., Elsevier, 517-541.
- , W. J. Hurlin, and A. D. Siegel, 1987: Simulation of the seasonal cycle of the tropical Pacific Ocean. *J. Phys. Oceanogr.*, **17**, 1986-2002.
- Ramanathan, V., 1987: Atmospheric general circulation and its low-frequency variance: Radiative influences. *Short and Medium-Range Weather Prediction*, T. Matsuno, Ed., 151-175.
- Randall, D. A., J. A. Abeles, and T. G. Corsetti, 1985: Seasonal simulations of the planetary boundary layer and boundary-layer stratocumulus clouds with a general circulation model. *J. Atmos. Sci.*, **42**, 641-676.
- Robertson, A. W., C.-C. Ma, C. R. Mechoso, and M. Ghil, 1994a: Simulation of the tropical-Pacific climate with a coupled ocean-atmosphere general circulation model. Part I: The seasonal cycle. *J. Climate*, in press.
- , —, M. Ghil, and C. R. Mechoso, 1994b: Simulation of the tropical-Pacific climate with a coupled ocean-atmosphere general circulation model. Part II: Interannual variability. *J. Climate*, in press.
- Rodgers, C. D., 1968: Some extensions and applications of the new random model for molecular band transmission. *Quart. J. Roy. Meteor. Soc.*, **94**, 99-102.
- Rosatì, A., and K. Miyakoda, 1988: A general circulation model for upper ocean simulation. *J. Phys. Oceanogr.*, **18**, 1601-1626.
- Schlesinger, M. E., 1976: A numerical simulation of the general circulation of atmospheric ozone. Ph.D. dissertation, University of California, Los Angeles, 376 pp.
- Suarez, M. J., A. Arakawa, and D. A. Randall, 1983: The parameterization of the planetary boundary layer in the UCLA general circulation model: Formulation and results. *Mon. Wea. Rev.*, **111**, 2224-2243.